Journal of Luminescence 225 (2020) 117372

Contents lists available at ScienceDirect

Journal of Luminescence

journal homepage: http://www.elsevier.com/locate/jlumin

1045 nm purely gain coupled semiconductor laser based on periodic electric injection

De-Zheng Ma [a,b], Yong-Yi Chen [a,c,*], Yu-Xin Lei [a,c,**], Peng Jia [a,***], Feng Gao [a,b], Yu-Gang Zeng [a,c], Lei Liang [a], Yue Song [a], Chun-Kao Ruan [a,b], Xia Liu [a,b], Li Qin [a,c], Yong-Qiang Ning [a], Li-Jun Wang [a,c]

[a] State Key Laboratory of Luminescence and Application, Changchun Institute of Optics, Fine Mechanics and Physics, Chinese Academy of Sciences, Changchun, 130033, China
[b] University of Chinese Academy of Sciences, Beijing, 100049, China
[c] Peng Cheng Laboratory, No.2, Xingke 1st Street, Nanshan, Shenzhen, China

ARTICLE INFO

Keywords:
Distributed feedback (DFB) laser
Periodic electric injection
Purely gain coupled

ABSTRACT

Distributed feedback lasers near 1050 nm have many applications such as high resolution imaging in medical, production inspection and 3-D sensing. In this paper, we demonstrate a purely gain coupled distributed feedback laser based on periodic electric injection. By using simple fabrication process steps, the same as those for Fabry–Perot lasers except for periodic current injection windows, we realized lasing single longitude mode in F–P structure due to surface periodic electric injection only. The device operates with a single-mode CW output of 51.9-mW power at 250 mA. The slope efficiency is 0.24 W/A, and the side-mode suppression radio is greater than 35 dB. The spectra maintain good single-mode output characteristics over a tuning range greater than 3.48 nm within only 9 °C.

1. Introduction

Distributed feedback laser diodes (DFB-LDs), having the advantages of small size and stable single-mode operation, have attracted widespread attention and are widely used in optical communication systems [1], integrated optical circuits and pumping sources for Erbium doped fiber (EDFA) lasers [2], etc. Because of their good single-mode operation properties and directly tuneable characteristics [3], DFB lasers have been seen as a promising candidate for the light sources in laser communication systems [4] and photonic integrated devices [5]. 1045 nm DFB-LDs are especially, ideal for spectroscopy, interferometry, high resolution imaging in medical and production inspection, as well as for 3-D sensing, LiDAR, and swept source optical coherence tomography (SS-OCT) [6]. In these cases, wide wavelength tunability is the first concern, and DFB-LD lasers can well satisfy the application of tunable laser field. With the introduction of mode-selective gating structures, two modified mechanisms for DFB-LD operation were introduced [7]. One of these is index-coupling DFB-LD operation, in which the real part of the reflective index is modulated to realize the laser output. However, the introduction of a uniform grating will cause the problem of degeneracy of two modes symmetric to the Bragg frequency [8]. Although there are some methods for solving this problem, such as introducing a phase shift to the grating [9] and asymmetrical facet coating [10], these approaches introduce additional problems. Phase-shifted gratings suffer from spatial hole burning effects if the laser diode is operated at high power, which results in reduced side-mode suppression ratio (SMSR) and quantum efficiency [11]. Asymmetrical facet coatings suffer from random facet phases introduced by cleavage, and this will decrease the single-mode yield [10].

Instead of index-coupling DFB-LD, gain coupled DFB-LD (brought up by Prof. K. Tada's group in Tokyo University) occurs by introducing a periodic change of gain (or loss) to modulate the imaginary part of

* Corresponding author. State key Laboratory of Luminescence and Application, Changchun Institute of Optics, Fine Mechanics and Physics, Chinese Academy of Sciences, Changchun, 130033, China.
** Corresponding author. State key Laboratory of Luminescence and Application, Changchun Institute of Optics, Fine Mechanics and Physics, Chinese Academy of Sciences, Changchun, 130033, China.
*** Corresponding author.
E-mail addresses: chenyy@ciomp.ac.cn (Y.-Y. Chen), leiyuxin@ciomp.ac.cn (Y.-X. Lei), jiapeng@ciomp.ac.cn (P. Jia).

https://doi.org/10.1016/j.jlumin.2020.117372
Received 29 October 2019; Received in revised form 11 May 2020; Accepted 12 May 2020
Available online 19 May 2020

reflective index and finally realize single-mode laser output exactly at the Bragg frequency [12]. In other words, gain coupled DFB-LD is inherently single-mode [8]. Moreover, gain coupled DFB-LD has the advantages facet immunity [13,14], insensitivity to external feedback [15], and easy integration using taper structures [16,17]. However, the realization required the introduction of etched active region [18]or periodic absorption grating [19], either affected the stability or suffered from higher threshold currrent and lower efficiency. The built-in grating structure still brought in index coupled effected even though may be compensated by multile complex grating structure [20]. Meanwhile, the manufacture of DFB-LD still requires the use of nanoscale grating fabrication technology and secondary material regrowth steps [21,22].

In our previous studies, we proposed a novel gain coupled DFB laser structure based on high-order periodic electric injection realized by periodically etched isolation grooves [23–25] to avoid nanoscale grating fabrication and secondary epitaxy. However, the introduction of etched grooves means that high-order photon diffraction, which causes power loss and a rise in the threshold, is inevitable [23]. To further optimize this structure, in this paper, we propose a purely gain coupled DFB-LD without any built-in grating structure. DFB single mode operation is realized in an Fabry–Perot (F–P) cavity based on periodic surface electric injection windows that modulate the imaginary part of reflective index, which will remove the fabrication of built-in grating structure, thus reducing the threshold current and improving output power and slope efficiency, as well as making the cavity without any inherent index coupling effect to be purely gain coupled. Furthermore, compared with formal works [26,27], our suggested approach didn't introduce any etched surface grating structures, the step of material etching can be reduced, which means we simpler fabrication method. Meanwhile, we have better performances such as lower threshold current and higher slope efficient since none high order diffraction loss was introduced. The devices were designed with periodic electric injection windows (6.12-μm period) in a 1-mm length of cavity and a 4-μm ridge width, and their fabrication requires the same steps as that of Fabry–Perot (F–P) lasers. Our devices realize single-mode laser outputs under all operation currents and temperatures, and their SMSR values is over 35 dB. The waveguide structure was just the same as F–P lasers, except for the help of periodic surface current injection windows only. A same production procedure as F–P laser was adopted, without nanoscale grating fabrication or secondary material regrowth. These devices exhibit threshold current of 40 mA, slope efficiency of 0.24 W/A, and power of 51.9 mW, and the minimum linewidth is 1.12 p.m. Thanks to their simplicity and low cost, the new scheme we proposed has great potential to be widely applied in commercial DFB products.

2. Structure design

A schematic diagram of the designed device structure is shown in Fig. 1(a). The GaAs substrate is at the bottom of the structure and the active region is sandwiched between the P-AlGaAs and N-AlGaAs waveguides. The p-cladding is directly beneath the periodic surface electrodes that are etched onto the ridge of the insulation layer. Ohmic contact electrodes were also fabricated.

In order to realize single-mode transmission, we simulated the mode-field distribution using COMSOL software. The 4-μm ridge width and 1.8-μm etching depth allow the waveguide to satisfy the conditions for single-transverse-mode operation. Fig. 1(b) shows the results of the simulation.

The carrier injection distribution of the device is shown in Fig. 2 (a): as can be observed, when current is injected, the carrier concentrations can be fitted by a sine function in the active region [28,29]. In this way, a periodic gain difference is induced within the active region, resulting in a periodic modulation of the imaginary part of the refractive index [30].

We simulated the carrier concentration distribution in quantum wells using PICS3D software. The results of the simulation with a 200-mA current injection are shown in Fig. 2(b). The hole distribution

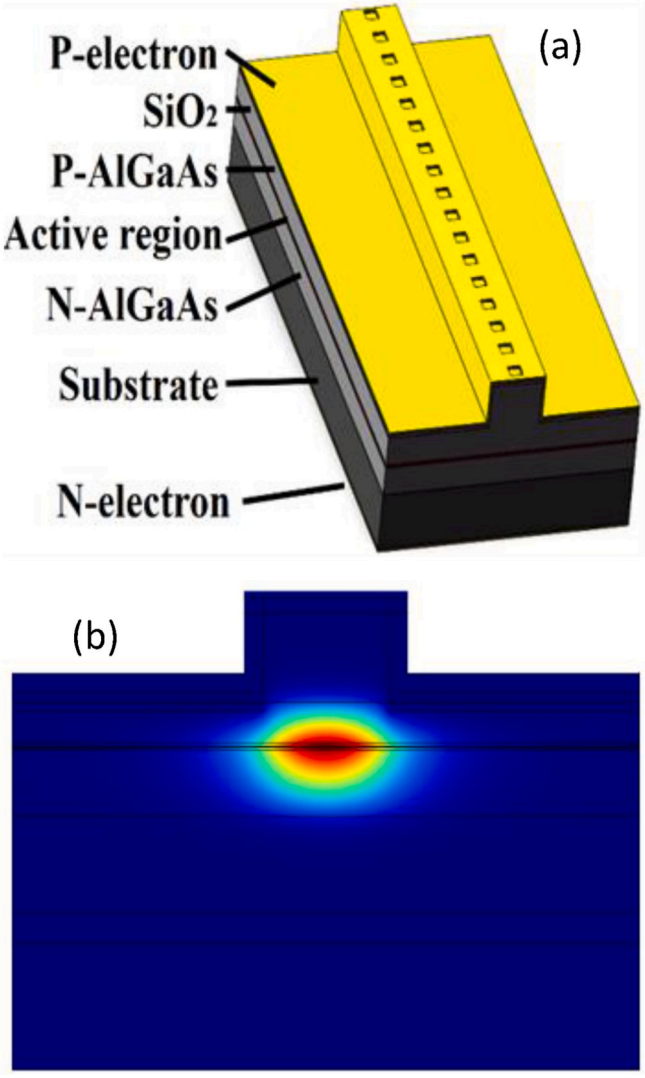

Fig. 1. Schematics of the purely gain coupled DFB laser. (a) Device structure. (b) Schematic diagram of simulation results. Ridge width is 4 μm, and etching depth is 1.8 μm.

along the cavity within the quantum well fits a sine function and the fitted result is

$$y = 2.46 + 0.14 * \sin((x - 1.54) / 2.98) \quad (1)$$

We can obtain the maximum and minimum values of carrier concentration C_1 and C_2 (shown in Fig. 2(b)). The corresponding gains, obtained using PICS3D (Fig. 3(a)), g_1 and g_2 at 1045 nm, are 1869.55cm^{-1} and 1657.217cm^{-1}, respectively; the difference in the gain contrast is $\Delta g = 212.3328 cm^{-1}$. According to Refs. [23],

$$\kappa = k_0 \Gamma^* \left(\Delta n + i \frac{\Delta g}{4 k_0} \right) \quad (2)$$

where Γ is the optical confinement factor and its value is 1.35%, as simulated by COMSOL.

Because there is no built-in grating structure in our device, the only index-coupling effects arise from the free-carrier-concentration induced material change within the quantum well, as shown in Fig. 2(b) and obtained using PICS3D, and imaginary part $\kappa L = 0.0717$, which can characterize the strength of the gain coupling. Using PICS3D, we simulated the gain spectrum according to different carrier density. Then we simulated the carrier density for the peak and the valley of the

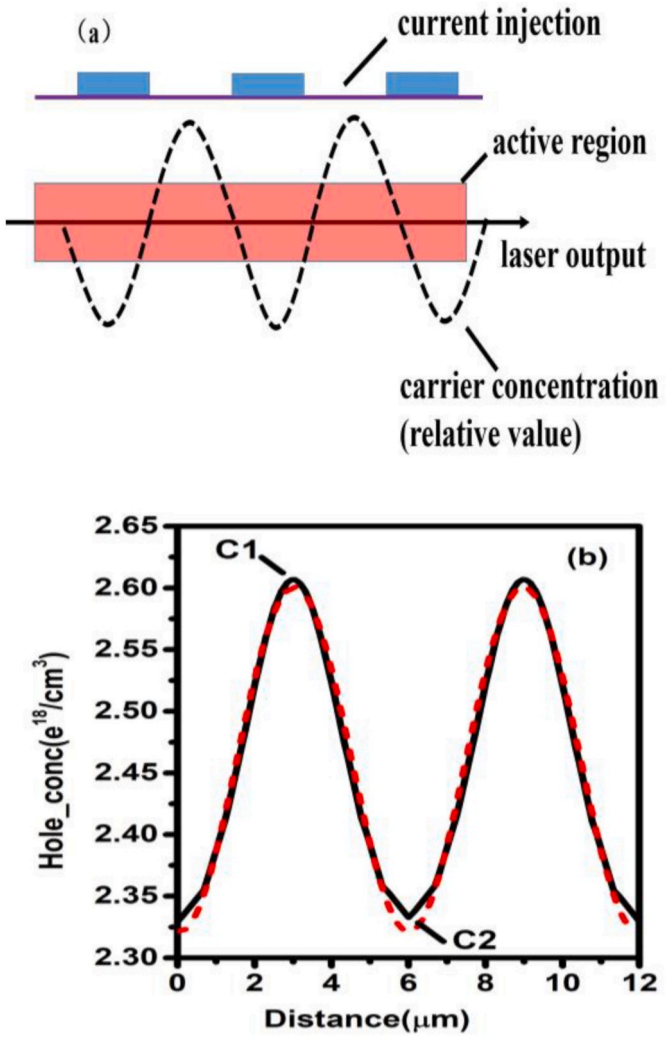

Fig. 2. (a) Schematic of cross section for periodic electric injection. (b) Simulated carrier concentration in quantum well.

quantum under different injection currents. Then we can get the gain difference versus injection current and calculate the gain coupling strength κL. The relation curve of imaginary of κL and injection current is shown in Fig.4, the reason for κL's gradual decrease is that, when the current density rises, the gain doesn't go linear any more; meanwhile the carrier density in the peak region tends to research gain saturation while the valley region still manages to rise as the current density rises, which causes the gain difference reduction.

We simulated the mode effective index n_{eff1} and n_{eff2} at C_1 and C_2 using the material index change of the quantum well; Δn_1 and Δn_2 are drawn from Fig. 3(b). The difference in the real part of the effective mode index is $\Delta n = 2.8 \times 10^{-6}$ ($n_{eff1} = 3.44185927$ and $n_{eff2} = 3.44186213$) and the real part $\kappa L = 2.2728 \times 10^{-4} << 1$, which can be used to characterize the strength of index-coupling and therefore may be omitted. As the imaginary part of κL is much larger than its real part, it can be considered that only the gain coupled mechanism is active, and hence for this device, the index-coupling mechanism need not be further considered [7]. Because the gain coupled effect was so weak that, it only helped picking out one of the FP modes into lasing. On the other hand, as can be seen from our test results below, even though the gain coupled effect was weak, it still managed to maintain our device to behave single longitudinal mode over the whole testing range.

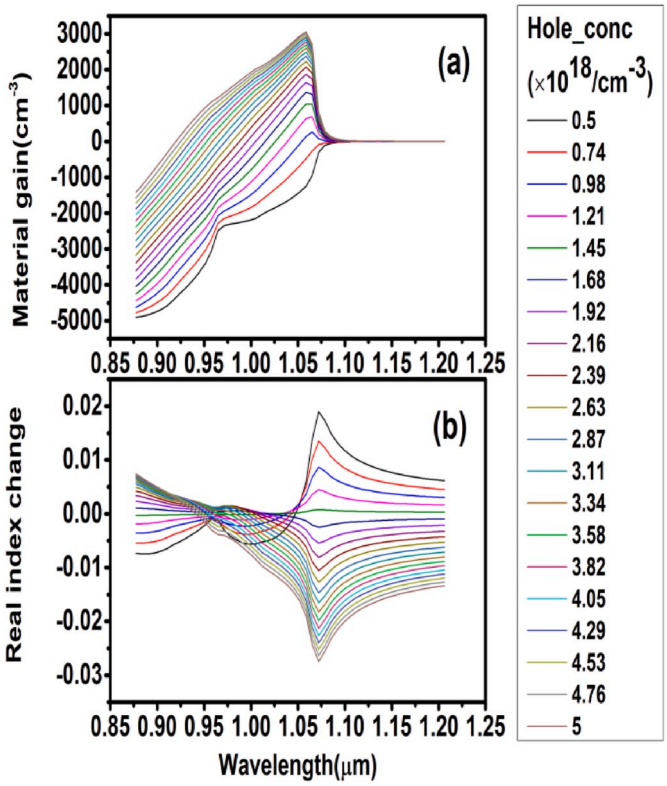

Fig. 3. PICS3D simulation results. (a) Material gain vs. wavelength. (b) Material index variation of the real part of QW.

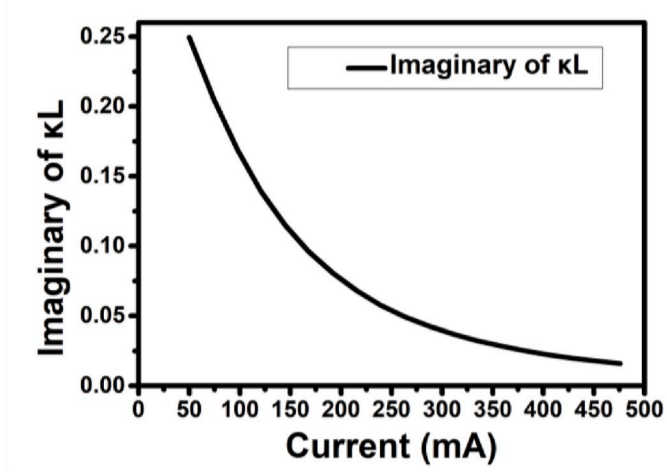

Fig. 4. Calculated curve of imaginary κL versus injection current.

3. Device fabrication

The key fabrication steps for these devices include material epitaxy, ridge etching, insulation-layer deposition, periodic electrode patterning, metallization, and chip packaging. The wafer we used was grown by metal–organic chemical-vapor deposition (MOCVD) on an n-type GaAs substrate. A ridge of 4 μm in width was patterned by photolithography and etched using an inductively coupling plasma (ICP) machine. The silica layer was grown by plasma-enhanced chemical vapor deposition (PECVD), and the periodic electron windows were made by conventional i-line photolithography. After ohmic contact on the surface of the wafer, the chip was cleaved into 1-mm-length devices, and coated on both sides; on one side with a high-reflective (HR) film (>99%) and on

the other with an anti-reflective (AR) film (<3%). Then the devices were mounted onto AlN ceramic submounts and placed on a water-cooled plate for further tests.

4. Results and discussion

The typical PIV (power vs. current vs. voltage) characteristics of the device during continuous-wave (CW) operation at 17 °C are shown in Fig. 5. The threshold current of the device is 40 mA, and the slope efficiency is 0.24 W/A. The power at 250 mA is 51.9 mW, and the power curve is very smooth without obvious discontinuities, jumps, or shifts in its slope.

The spectrum of the device at 220 mA CW is shown in Fig. 6, at a temperature of 17 °C. Under these circumstances, the central wavelength of the spectrum is 1044.81 nm, and the highest side-mode suppression ratio (SMSR) at this temperature is 37.3 dB. The spectrum retains its single-mode character and the SMSR value is >35 dB at other operating temperatures and currents.

As shown in Fig. 7, the measured 3-dB spectral linewidth of the narrowband single-mode emission, measured by F–P interferometer, is less than 1.15 p.m. The linewidth was measured by coupling the collimated laser to the F–P interferometer (Thorlabs, SA200-8B), which has a resolution of 67 MHz and free spectral range of 10 GHz. The linewidth is calculated as

$$\Delta\nu = (t_{FWHM} / \Delta t)^* \nu_0 \quad (3)$$

where t_{FWHM} is the full width at half maximum of the scanned spectrum, Δt is the interval between the scanned spectrum, and ν_0 is the free spectral range. The 3-dB spectral linewidth of our device is much narrower than that of our previously reported DFB laser which has a spectral linewidth of 3.2 pm [23].

By changing the water-cool conditions, spectra at different temperatures may be recorded, and are shown in Fig. 8. Fig. 8(a), (b), (c), and (d) show the spectra at 120 mA, 180 mA, 230 mA, and 240 mA, respectively; the inset panels show individual plots measured at 17 °C. The central wavelength of the device is red shifted when the temperature increases, while the spectra retain their single-mode characteristic.

The spectra at different currents are shown in Fig. 9 at temperatures of 18 °C, 20 °C, 24 °C, and 25 °C, respectively shown in Fig. 9(a), (b), (c), and (d). It is apparent in Fig. 8 that the central wavelengths gradually increase as the current (CW) increases, and the largest SMSR is 38 dB, which was obtained at 240 mA with a water-cooling temperature 18 °C (inset, Fig. 9(a)). It should be mentioned that at each investigated combination of operating temperature and current, the spectrum was demonstrated to be stable and repeatable. Nonetheless, when

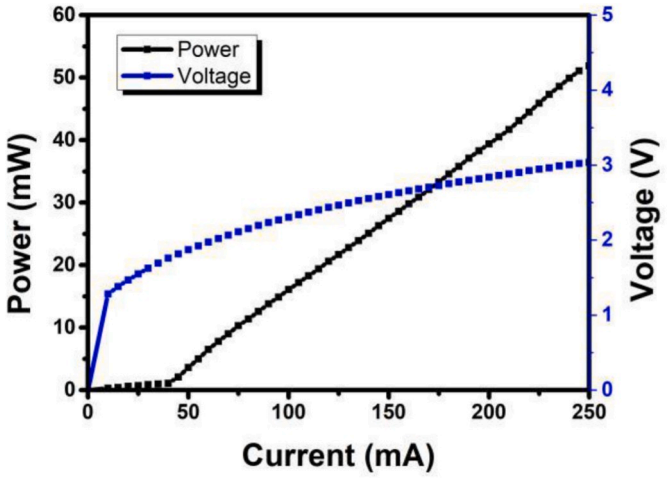

Fig. 5. PIV characteristics at 17 °C.

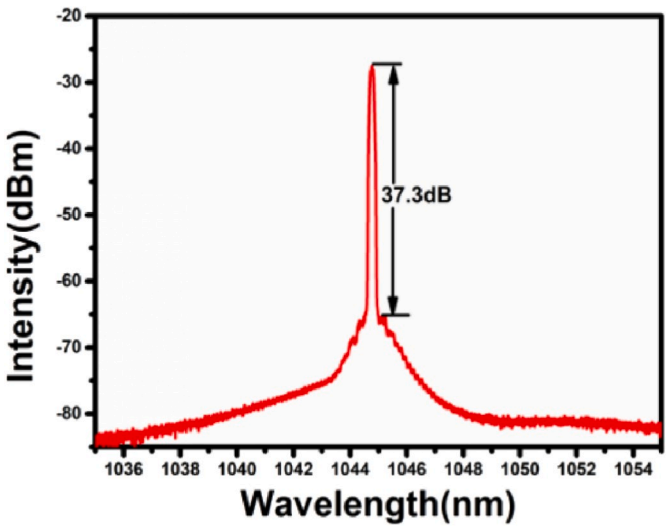

Fig. 6. Spectrum of the device at 220 mA.

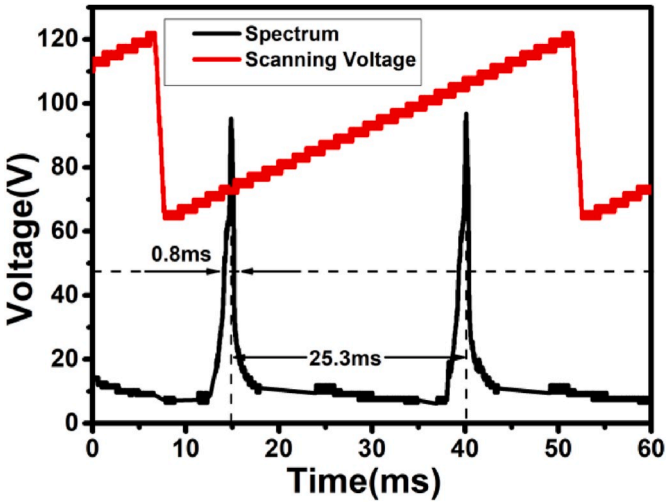

Fig. 7. Linewidth pattern of device at 200 mA.

temperature or current changes, the spectrum exhibits discontinuity and hops from one mode to another. Fig. 10 shows the behavior of the central wavelength as operating current increases at different temperatures. The phenomenon of mode hopping can be clearly observed. The final quasi-continuous tuning range realized was 3.48 nm.

The reason for the red-shifting of the central wavelength is because the device is placed on the water-cooling plate and the water temperature is the only temperature control, therefore the quantum well will accumulate heat and a temperature rise will occur for larger current injections; the gain spectrum will red shift as the temperature rises.

The mode hopping is caused by the two following reasons. The main reason is the F–P effect brought by the coating films. The light emitting facet of the device is coated with an AR film (<3%), and the other facet is coated with a HR film (>99%). This film coating is not sufficient to eliminate F–P phenomena caused by the facets. As the temperature rises and the current density changes, the gain spectrum shifts and when the eigen Bragg DFB frequency shifts match the interval modes of the F–P filter, the lasing spectrum tends to hop between F–P filter modes because of mode competition. Moreover, the water-cooling machine used to change the temperature of the cooling water from 16 to 25 °C is not sufficiently accurate to measure the actual working temperature of the chip and therefore additional unmeasured temperature fluctuations may

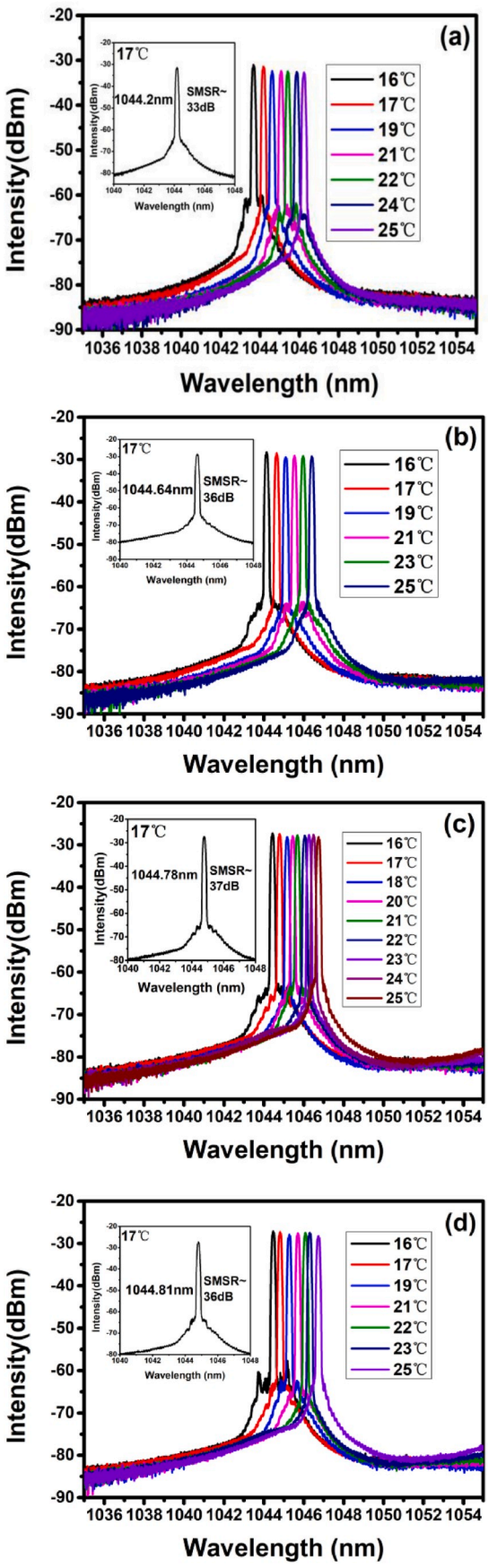

Fig. 8. Spectra at different temperatures. (a) 120 mA. (b) 180 mA. (c) 230 mA. (d) 240 mA.

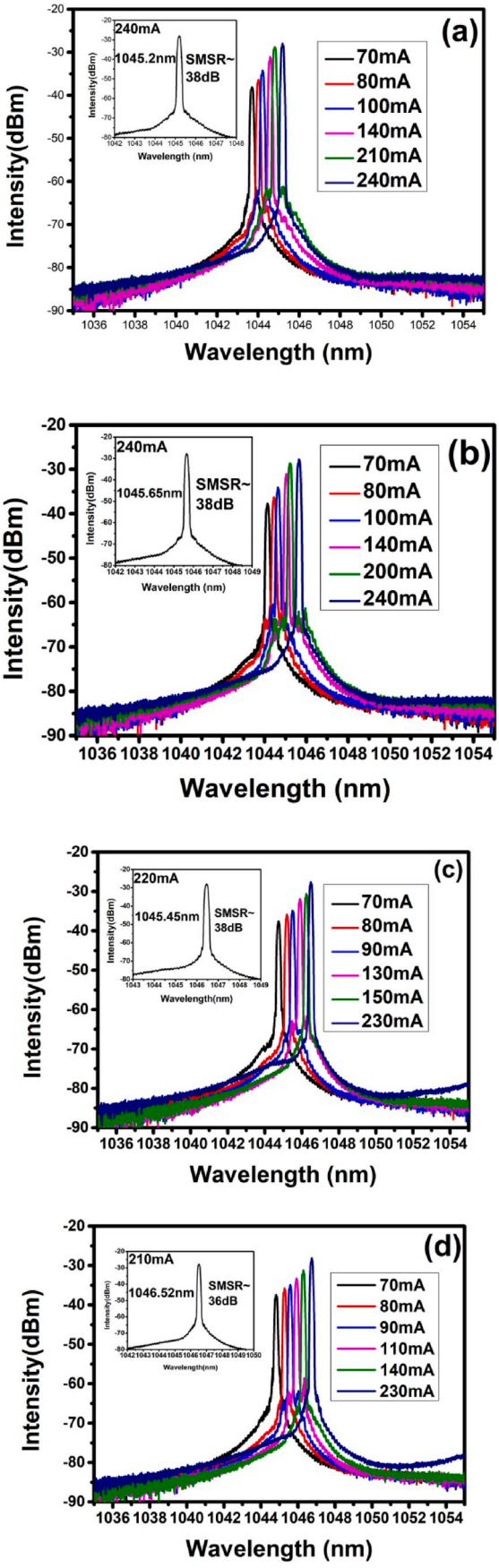

Fig. 9. Spectra at different currents. (a)18 °C. (b)20 °C. (c)24 °C. (d) 25 °C.

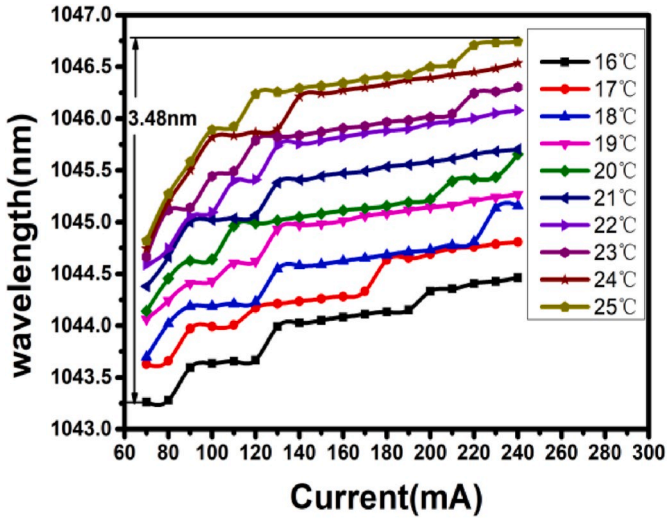

Fig. 10. Central lasing wavelength changes with increasing operating current at different temperatures.

also cause some mode hopping.

Comparing with our previous study [23], the device without etching grooves has a greatly simplified fabrication: the same as an F–P laser. And high order diffraction loss has been eliminated. Even though the gain contrast is smaller, the spectrum SMSR is still larger 35 dB for all testing currents. And single longitude mode lasing reached over 50 mW for more than 37 dB, this is an obvious evident that the gain coupled effect is the dominant factor, although F–P mode are responsible for the mode hopping during tuning. The F–P modes could be further removed by better film coating (AR reflectivity $< 0{,}1\%$, or AR coatings on both sides of the cavity) or titled emitting ends.

5. Conclusion

In this paper, we demonstrated a DFB laser in an F–P structure, and only periodic surface current injection windows are utilized. Through the periodic electric injection windows, we realized purely gain coupled DFB lasing without introducing any grating structures. Stable single mode laser working at 1045 nm based on periodic electric injection was demonstrated. The single-mode CW operation output power is 51.9 mW at 250 mA, the slope efficiency is 0.24 W/A, and the SMSR is >35 dB for the entire test range from 40 mA (at the threshold) to 240 mA, and the highest SMSR is 38 dB, which occurs at 240 mA, with water cooling temperature at 18 °C. The spectra maintain good single-mode output characteristics at all operating temperatures and current-injection conditions in our tests. The total tuning range is larger than 3.48 nm for only 9 °C water cooling range. Our technique is a promising candidate for practical applications in laser communication and optical integration of single longitude mode lasers.

Declaration of competing interest

There are no conflicts of interest.

Acknowledgement

This work is supported by National Science and Technology Major Project of China (2018YFB2200300); Frontier Science Key Program of the President of the Chinese Academy of Sciences (QYZDY-SSW-JSC006); National Natural Science Foundation of China (NSFC) (11874353, 61935009, 61934003, 61604151, 61674148, 61904179, 61727822, 11604328, 61805236); Youth Program of National Natural Science Foundation of China(61904179), Dawn Talent Training Program of CIOMP.

References

[1] Y. Liu, L. Ju, X.L. Liang, S.B. Tang, G.L. Tu, L. Zhou, C.Z. Peng, K. Chen, T.Y. Chen, Z.B. Chen, Experimental demonstration of counterfactual quantum communication, Phys. Rev. Lett. 109 (2012), 030501, https://doi.org/10.1103/PhysRevLett.109.030501.

[2] M. Horiguchi, K. Yoshino, M. Shimizu, M. Yamada, Highly efficient optical fibre amplifier pumped by a 0.8 μm band laser diode, Electron. Lett. 29 (1993) 593–595, https://doi.org/10.1049/el:19901129.

[3] Amin Abbasi, Leili Abdollahi Shiramin, Bart Moeneclaey, Jochem Verbist, Xin Yin, Johan Bauwelinck, Dries Van Thourhout, Roelkens Gunther, Geert Morthier, III-V-on-Silicon C-band high-speed electro-absorption modulated DFB laser, J. Lightwave Technol. 36 (2018) 252–257, https://doi.org/10.1109/JLT.2017.2743044.

[4] Andrei P. Bakoz, Alexandros A. Liles, Alfredo A. Gonzalez-Fernandez, Tatiana Habruseva, Changyu Hu, Evgeny A. Viktorov, Stephen P. Hegarty, Liam O'Faolain, Wavelength stability in a hybrid photonic crystal laser through controlled nonlinear absorptive heating in the reflector, Light Sci. Appl. 7 (2018), https://doi.org/10.1038/s41377-018-0043-8.

[5] Zhiping Zhou, Bing Yin, Jurgen Michel, On-chip light sources for silicon photonics, Light Sci. Appl. (2015) 4, https://doi.org/10.1038/lsa.2016.98.

[6] N. Abroug, I. Ksiaa, M. Lupidi, W. Nabi, S. Attia, B. Jelliti, S. Khochtali, M. Khairallah, Swept source-OCT and swept source-OCT angiography findings in posterior microphthalmos", Int. Ophthalmol. (2019) https://doi.org/10.1007/s10792-019-01115-7.

[7] K. David, G. Morthier, P. Vankwikelberge, R.G. Baets, T. Wolf, B. Borchert, Gain-coupled DFB lasers versus index-coupled and phase-shifted DFB lasers: a comparison based on spatial hole burning corrected yield, IEEE J. Quant. Electron. 27 (6) (1991) 1714–1723, https://doi.org/10.1109/3.89938.

[8] H. Kogelnik, C.V. Shank, Coupled-wave theory of distributed feedback lasers, J. Appl. Phys. 43 (5) (2008) 2327–2335, https://doi.org/10.1063/1.1661499.

[9] S. Nilsson, T. Kjellberg, T. Klinga, R. Schatz, J. Wallin, K. Streubel, Improved spectral characteristics of MQW-DFB lasers by incorporation of multiple phase-shifts, J. Lightwave Technol. 13 (1995) 434–441, https://doi.org/10.1109/50.372439.

[10] S.R. Chinn, Effects of mirror reflectivity in a distributed-feedback laser, IEEE J. Quant. Electron. 9 (6) (1973) 574–580, https://doi.org/10.1109/JQE.1973.1077551.

[11] H. Soda, Y. Kotaki, H. Sudo, H. Ishikawa, Stability in single longitudinal mode operation in GaInAsP/InP phase-adjusted DFB lasers, IEEE J. Quant. Electron. 23 (6) (1987) 804–814, https://doi.org/10.1109/JQE.1987.1073454.

[12] Y.Y. Chen, P. Jia, J. Zhang, H. Chen, F. Gao, X. Zhang, X.N. Shan, Y.Q. Ning, L. J. Wang, L. Qin, Gain-coupled distributed feedback laser based on periodic surface anode canals, J. Appl. Mech. 82 (10) (2015) 8863–8866, https://doi.org/10.1364/AO.54.008863.

[13] S.T. Kim, B.G. Kim, Analysis of single-mode yields above threshold for complex coupled distributed feedback lasers with asymmetric facet reflectivities, J. Opt. Soc. Am. B 22 (5) (2005) 1010–1015, https://doi.org/10.1364/JOSAB.22.001010.

[14] N. Susa, Fluctuations of the laser characteristics and the effect of the index-coupling component in the gain-coupled DFB laser, IEEE J. Quant. Electron. 33 (1997) 2255–2265, https://doi.org/10.1109/3.644108.

[15] A.J. Lowery, D. Novak, Performance comparison of gain-coupled and index-coupled DFB semiconductor lasers, IEEE J. Quant. Electron. 30 (9) (1994) 2051–2063, https://doi.org/10.1109/3.309864.

[16] Y.X. Lei, Y.Y. Chen, F. Gao, D.Z. Ma, P. Jia, Q. Cheng, H. Wu, C.K. Ruan, L. Liang, C. Chen, J. Zhang, J.Y. Tian, L. Qin, Y.Q. Ning, L.J. Wang, 990 nm high-power high-beam-quality DFB laser with narrow linewidth controlled by gain-coupled effect, IEEE Photonics Jounal 11 (1) (2019) 1–9, https://doi.org/10.1109/JPHOT.2019.2893961.

[17] Y.X. Lei, Y.Y. Chen, F. Gao, D.Z. Ma, P. Jia, H. Wu, C. Chen, L. Liang, J. Zhang, J. Y. Tian, L. Qin, Y.Q. Ning, L.J. Wang, High-power single-longitudinal-mode double-tapered gain-coupled distributed feedback semiconductor lasers based on periodic anodes defined by i-line lithography, Optic Commun. 443 (2019) 150–155, https://doi.org/10.1016/j.optcom.2019.02.073.

[18] K. Tada et al., United State Patent, Patent Number 5077752.

[19] Y. Luo, H.-L. Cao, M. Dobashi, H. Hosomatsu, K. Tada, Y. Nakano, GaAlAs/GaAs single quantum well gain-coupled distributed feedback laser, IEEE Photon. Technol. Lett. 3 (12) (1991) 1052–1054, https://doi.org/10.1109/68.117997.

[20] Y. Luo, H.-L. Cao, M. Dobashi, H. Hosomatsu, Y. Nakano, K. Tada, Gain-coupled distributed feedback semiconductor lasers with an absorptive conduction-type inverted grating, IEEE Photon. Technol. Lett. 4 (7) (1992) 692–695, https://doi.org/10.1109/68.145240.

[21] R.J. Guo, J. Lu, S.P. Liu, Y.C. Shi, Y.T. Zhou, Y.T. Chen, J. Luan, X.F. Chen, Multisection DFB tunable laser based on REC technique and tuning by injection current, IEEE Photonics Journal 8 (4) (2016) 1–7, https://doi.org/10.1109/JPHOT.2016.2585923.

[22] Y. Shi, S. Li, R. Guo, R. Liu, Y. Zhou, X. Chen, A novel concavely apodized DFB semiconductor laser using common holographic exposure, Optic Express 21 (13) (2013) 16022–16028, https://doi.org/10.1364/OE.21.016022.

[23] F. Gao, L. Qin, Y.Y. Chen, P. Jia, C. Chen, L.W. Cheng, H. Chen, L. Liang, Y.G. Zeng, X. Zhang, Study of gain-coupled distributed feedback laser based on high order surface gain-coupled gratings, Optic Commun. 410 (2018) 936–940, https://doi.org/10.1016/j.optcom.2017.09.023.

[24] F. Gao, L. Qin, Y.Y. Chen, P. Jia, C. Chen, H. Chen, L. Liang, Y.G. Zeng, X. Zhang, Y. Q. Ning, two-segment gain-coupled distributed feedback laser, IEEE Photonics Journal 10 (1) (2018) 1–9, https://doi.org/10.1109/JPHOT.2018.2791610.
[25] F. Gao, L. Qin, Y.Y. Chen, P. Jia, C. Chen, L.W. Cheng, H. Chen, L. Liang, Y.G. Zeng, X. Zhang, Narrow-strip single-longitudinal-mode laser based on periodic anodes defined by i-line lithography, IEEE Photonics Journal 10 (2) (2018) 1–10, https://doi.org/10.1109/JPHOT.2018.2818170.
[26] A. Abdullaev, Q. Lu, W. Guo, M.J. Wallace, M. Nawrocka, F. Bello, Improved performance of tunable single-mode laser array based on high-order slotted surface grating, Optic Express 23 (9) (2015) 12072–12078, https://doi.org/10.1364/OE.23.012072.
[27] J. Fricke, H. Wenzel, F. Bugge, O.P. Brox, A. Ginolas, W. John, G. Erbert, High-power distributed feedback lasers with surface gratings, IEEE Photon. Technol. Lett. 24 (16) (2012) 1443–1445, https://doi.org/10.1109/LPT.2012.2206378.
[28] S.L. Chuang, Physics of Photonic Devices, Wiley, 2009.
[29] Hans Wenzel, Jörg Fricke, Jonathan Decker, Crump Paul, Götz Erbert, High-power distributed feedback lasers with surface gratings: theory and experiment, IEEE J. Sel. Top. Quant. Electron. 21 (6) (2015), https://doi.org/10.1109/JSTQE.2015.2429892.
[30] M. Ito, T. Kimura, Carrier density dependence of refractive index in AlGaAs semiconductor lasers, IEEE J. Quant. Electron. 16 (9) (1980) 910–911, https://doi.org/10.1109/JQE.1980.1070603.